New buffer layer material La(Pr)CrO_3 for intermediate temperature solid oxide fuel cell using $LaGaO_3$-based electrolyte film

Young-Wan Ju, Jong-Eun Hong, and Junji Hyodo
Department of Applied Chemistry, Faculty of Engineering, Kyushu University, Nishi-Ku, Fukuoka 819-0395, Japan

Toru Inagaki
The Kansai Electric Power Co., Inc., Amagasaki, Hyogo 661-0974, Japan

Shintaro Ida and Tatsumi Ishihara[a)]
Department of Applied Chemistry, Faculty of Engineering, Kyushu University, Nishi-Ku, Fukuoka 819-0395, Japan

(Received 12 January 2012; accepted 21 May 2012)

A metal-supported solid oxide fuel cell (SOFC) using $Ce_{0.8}Sm_{0.2}O_2$ (Sm-doped ceria, SDC) buffer layer and $La_{0.9}Sr_{0.1}Ga_{0.8}Mg_{0.2}O_3$ (LSGM) electrolyte films showed a small degradation in the cell performance after a long-term operation because of La migration from the electrolyte to the buffer layer, resulted in a formation of a less conductive phase. Thus, various ceramic materials such as doped ceria and perovskite-related oxides were investigated for an effective buffer layer with respect to fabricating reliable metal-supported SOFCs using a LSGM electrolyte film. In particular, La-doped CeO_2 (LDC) and Pr-doped $LaCrO_3$ (LPCr) were investigated as buffer layer material since the materials showed chemical compatibility with the LSGM and anode materials. The cell using a LDC buffer layer showed a prior stability during the operation for 100 h at 973 K, while the power density of the cell was slightly low owing to the low electrical conductivity of LDC compared with that of SDC or LPCr. In contrast, the cell using a LPCr buffer layer revealed significantly low open circuit voltage (OCV) and power density, which were attributed to Pr decomposition in the LPCr caused by the reactivity with water vapor. However, the metal-supported cell with a multilayer electrolyte film including LSGM/LPCr/SDC layers showed an almost theoretical OCV and reasonably high power density with no degradation after a long-term operation for 100 h at 973 K, suggesting that the LPCr layer effectively prevented La migration and the SDC layer led to avoid the Pr decomposition. Thus, a LPCr is an effective buffer layer material for reliable metal-supported SOFCs using a LSGM electrolyte thin film.

I. INTRODUCTION

Solid oxide fuel cells (SOFCs) are regarded as a promising power generation system due to the high-energy conversion efficiency comparing with that of other type fuel cells. In addition, SOFCs can use various fuels such as hydrocarbon or alcohol without a precious metal catalyst such as Pt.[1–3] The fuel flexibility is originated from the internal gas reforming, which is highly effective for improving the efficiency. However, materials used for SOFCs are limited by ceramics, and a long start-up period is requested due to the high operating temperature. Therefore, at present, there are many efforts to operate SOFCs at intermediate temperature, which is also effective for extending the application area of SOFCs. However, the power density and conversion efficiency significantly decrease with reducing the operation temperature because of the enlarged internal resistance (IR) of electrolyte. Various investigations have been focused on the discovery of a new electrolyte material[4–22] and the fabrication of a thin electrolyte film[15–26] to reduce the electrolyte resistance, which is mainly dominated by low conductivity and large thickness of electrolyte. Among new electrolyte materials, $La_{0.9}Sr_{0.1}Ga_{0.8}Mg_{0.2}O_{3-\delta}$ (LSGM) has been considered as an excellent electrolyte material for intermediate temperature solid oxide fuel cells (IT-SOFCs) because it has high oxide ionic conductivity at intermediate temperatures and high transference number of oxide ions over a wide range of oxygen partial pressures.[7–11] However, LSGM electrolyte has some drawbacks such as the reactivity with the electrode materials[11,12] and poor mechanical strength compared with that of Y_2O_3-stabilized ZrO_2.

We have introduced a Ni–Fe metal-supported SOFC having a thin LSGM electrolyte film to solve the problem for poor mechanical strength, in our previous study.[19–24] In addition, we confirmed that the reaction between the LSGM electrolyte and Ni in the anode was prevented by inserting a Sm-doped CeO_2 (SDC) thin buffer layer and decreasing the sintering temperature of the LSGM electrolyte film prepared by a pulsed laser deposition (PLD). The PLD is

a)Address all correspondence to this author.
e-mail: ishihara@cstf.kyushu-u.ac.jp
DOI: 10.1557/jmr.2012.187

 © Materials Research Society 2012

https://doi.org/10.1557/jmr.2012.187 Published online by Cambridge University Press

unique method to fabricate thin and uniform film at a lower temperature compared with other fabrication methods such as tape casting,[25] screen printing,[26] spin coating,[27] colloidal deposition,[28] plasma spraying,[29,30] electrostatic-assisted vapor deposition,[31] and physical vapor deposition.[32] Therefore, many research groups have adopted for fabricating SOFC having thin film despite of difficulty in the scale-up of cell size. The prepared metal-supported SOFC has exhibited high power density at intermediate temperatures (from 973 to 773 K) and good tolerances against thermal and redox cycling. However, after a long-term operation for 100 h, the cell performance has degraded because of the interdiffusion of La from the LSGM electrolyte to the SDC buffer layer. The diffused La forms a La-doped CeO_2 (LDC) in the SDC layer, which is known to have a lower conductivity than that of SDC. In addition, a secondary phase $LaSrGa_3O_7$ structure is produced in the LSGM electrolyte layer because of the La migration to the SDC layer resulting in the decrease of power generation property.[11,12] Therefore, an investigation on a new buffer layer for a LSGM electrolyte film is necessary for fabricating excellent and stable metal-supported IT-SOFCs.

In this study, we investigated various materials such as doped CeO_2, $SrTiO_3$, and $LaCrO_3$ as a buffer layer for metal-supported SOFCs using a LSGM thin electrolyte film prepared using the PLD method. Among materials studied, 40 mol% LDC and 19 mol% Pr-doped $LaCrO_3$ (LPCr) showed no reactivity with LSGM and Ni. Therefore, we further investigated long-term stability on metal-supported cells using the LDC or LPCr as buffer layer.

II. EXPERIMENT

A. Preparation of buffer layer materials

For development of a new buffer layer material, two kinds of approach were adopted. One is to modify doped CeO_2, particularly for 40 mol% LDC by codoping $[(Ce_{0.5}La_{0.4}M_{0.1})O_{2-\delta}$, M = Ga, Y, Pr, Nd, and Sm], which was prepared by a typical solid-state reaction (Table I). Another is to introduce mixed ionic and electronic conductors (MIECs) as a buffer layer. The MIEC materials were prepared by a typical solid-state reaction, sol–gel method, or impregnation method, respectively, as summarized in Table II. X-ray diffraction (XRD) using CuKα radiation (Rint 2500, Rigaku, Tokyo, Japan) was measured to determine phase formation of all prepared materials. To confirm the reactivity of a buffer layer material against NiO or LSGM, the prepared powder was mixed with commercial NiO or prepared LSGM in an agate mortar. After calcination of the mixture at 1623 K for 6 h, the reactivity was confirmed by powder XRD analysis. The electrical conductivity of each material was measured by using dc four-probe method with rectangular bar sample in air at the temperature rage of 673–1173 K. A Pt wire was connected to the conductivity sample with Pt paste. The activation energy of measured conductivity data was calculated using the Arrhenius equation as following:

$$\sigma T = \sigma_0 \exp\left(\frac{E_a}{kT}\right) \quad . \tag{1}$$

B. Fabrication of metal-supported cell and electrochemical measurements

Ten wt% Fe_2O_3-coated NiO powder was prepared by a traditional impregnation method. $Fe(NO_3)_3 \cdot 9H_2O$ was dissolved in deionized water, and then, NiO powder was added into the solution proportionately. After the evaporation of water, the obtained powder was calcined in a ventilated furnace at 673 K for 2 h to decompose nitrate acid and then fired at 1473 K for 6 h. To obtain a fine and uniform particle mixture, the mixed powder was ground for 1 h in ethanol using the ball milling process with zirconia balls. After drying the slurry, the resulting powder was pressed into disks (20 mm in diameter) at 20 MPa. After isostatically pressing at 48 MPa, the obtained disks were sintered at 1723 K for 5 h in air; the thickness of substrate was 1.7 mm.[21–23] Thin $La_{0.9}Sr_{0.1}Ga_{0.8}Mg_{0.2}O_3$ (LSGM) electrolyte and $Ce_{0.8}Sm_{0.2}O_2$ (SDC) buffer layer films were then deposited onto the dense anode substrate via the PLD method using a commercial system with a vacuum chamber (PLD-7, PASCAL, Itami, Japan). Before deposition, the substrate was heated to 1073 K with an infrared heater, and the oxygen pressure during deposition was adjusted to 0.67 Pa by introducing commercial oxygen without purification. The power and frequency of excimer laser were adjusted to 180 mJ/pulse and 10 Hz, respectively. Molar ratio of La, Sr, Ga, and Mg in optimized target for deposition of LSGM electrolyte was La:Sr:Ga:Mg = 0.7282:0.1:0.6380:0.4255. For fabricating a thin buffer layer film, each target disk having an optimized composition was prepared using a solid-state reaction as listed in Table III. A thin convex-shaped Sm-doped $SrCo_3$ (SSC) layer as the cathode was fabricated via the PLD method with an optimized SSC target composition on the thin LSGM film after postannealing in air at 1073 K for 2 h.[24] For preparing the SSC layer, target disk was fabricated by conventional solid-state reaction method using Sm_2O_3, $SrCO_3$, and Co_3O_4 as the starting materials. Molar ratio of the optimized target composition was Sm:Sr:Co = 0.4:0.6:1.6. The diameter of the deposited SSC layer was 5 mm. A SSC powder cathode (around 20 μm) was then prepared using a slurry coating method on the deposited SSC film and then fired at 1073 K for 30 min. A Pt wire was connected to the LSGM film near the cathode as the reference electrode.

The power generation property of a metal-supported cell was measured by the four-probe method. Humidified H_2 (2.8 vol% H_2O) and commercial oxygen were fed to the cell as fuel and oxidant, respectively. The gas flow rate

https://doi.org/10.1557/jmr.2012.187 Published online by Cambridge University Press

TABLE I. Summary of properties of co-doped ceria.

Composition	Synthesis	Secondary phase	Secondary phase (S/cm)
$Sm_{0.2}Ce_{0.8}O_{2-\delta}$ (SDC)	Commercial product	LDC	0.174
$La_{0.4}Ce_{0.6}O_{2-\delta}$ (LDC)	Impregnation	...	0.047
$La_{0.4}Ga_{0.1}Ce_{0.6}O_{2-\delta}$(LGC)	Solid state	$LaGaO_3$ (during the preparation)	0.019
$La_{0.4}Y_{0.1}Ce_{0.6}O_{2-\delta}$ (LYC)	Solid state	$LaSrGaO_4$	0.015
$La_{0.4}Pr_{0.1}Ce_{0.6}O_{2-\delta}$ (LPC)	Solid state	$LaSrGaO_4$	0.028
$La_{0.4}Nd_{0.1}Ce_{0.6}O_{2-\delta}$ (LNC)	Solid state	$LaSrGaO_4$	0.023
$La_{0.4}Sm_{0.1}Ce_{0.6}O_{2-\delta}$ (LSC)	Solid state	$LaSrGaO_4$	0.022

TABLE II. Summary of investigated materials for new buffer layer.

Composition	Synthesis	Secondary phase	Conductivity (at 1123 K) (S/cm)
$Sm_{0.2}Ce_{0.8}O_{2-\delta}$ (SDC)	Commercial product	La-doped CeO_3	0.129
$La_{0.4}Ce_{0.6}O_{2-\delta}$ (LDC)	Impregnation	...	0.030
$SrTio_3$	Solid state	Unknown and $La_2Sr_7TiO_{11}$	...
La_2NiO_4	Solid state	La_4NiO_{10} and La_3NiO_7	51.58
$La_2Zr_2O_7$	Sol–gel	Unknown and $SrZrO_3$	...
$Gd_{1.2}La_{0.8}Zr_2O_7$	Sol–gel	...	0.001
$Sm_2Zr_2O_7$	Sol–gel	Unknown	0.009
La_2TiO_7	Sol–gel	$La(Ni_{0.5}Ti_{0.5})O_3$ (reaction with NiO)	...
$SmFeO_3$	Thermal decomposition	$La_{0.9}Sm_{0.1}GaO_3$	...
$La_{0.8}Pr_{0.2}MnO_3$	Solid state	Ni_6MnO_8 (reaction with NiO)	130
$La_{0.9}Sr_{0.1}CrO_3$	Solid state	Unknown	...
$La_{0.8}Sr_{0.2}CrO_3$	Solid state	Unknown	...
$La_{0.9}Pr_{0.1}CrO_3$	Solid state	$LaSrGa_3O_7$	0.199
$La_{0.81}Pr_{0.19}CrO_3$	Solid state	...	0.310
$La_{0.8}Pr_{0.2}CrO_3$	Solid state	$LaSrGaO_4$	0.111

TABLE III. Fabrication condition for deposited film.

	Deposition conditions			
	Composition of target	Deposition rate (μm/min)	Substrate temperature (K)	
SDC (500 nm, $Sm_{0.2}Ce_{0.8}O_{2-\delta}$)	$Sm_{0.2}Ce_{0.8}O_{2-\delta}$	12.5	1073	
LDC (500 nm, $La_{0.4}Ce_{0.6}O_{2-\delta}$)	$La_{0.4}Ce_{0.6}O_{2-\delta}$	12.5	1073	
LPCr (500 nm, $La_{0.01}Pr_{0.19}CrO_{3-\delta}$)	$La_{0.71}Pr_{0.12}Cr_{1.22}O_{2-\delta}$	16.7	1073	180 mJ/Plus, 10 Hz, 0.67 Pa
LSGM (6 μm, $La_{0.9}Sr_{0.1}Ga_{0.8}Mg_{0.2}O_{3-\delta}$)	$La_{0.7282}Sr_{0.1}Ga_{0.6380}Mg_{0.4255}O_{3-\delta}$	10.4	1073	
SSC (500 nm, $Sm_{0.5}Sr_{0.5}CoO_{3-\delta}$)	$Sm_{0.4}Sr_{0.6}Co_{1.6}O_{3-\delta}$	16.7	298	

was kept to be 100 mL/min in this study. A constant current was applied by using a galvanostat (HA-301, Hokuto Denko, Tokyo, Japan), and the potential was measured with a digital multimeter (Digital Multimeter R6451A, Advantest, Tokyo, Japan). IR drop and overpotential were estimated by the current interruption method. A current pulse was generated with a current pulse generator (Current Pulse Generator HC111, Hokuto Denko, Tokyo, Japan) and the residual potential response was analyzed with a memory hicoder (Memory Hicoder 8835, Hioki, Nagano, Japan). Microstructure of the cell was studied using a scanning electron microscope (SEM, VE-7800; KEYENCE, Osaka, Japan)/energy dispersive x-ray spectroscopy (EDX) after the cell test.

III. RESULTS AND DISCUSSION

A. Investigation for codoped ceria

Figure 1 shows the power generating property of a metal-supported cell using a SDC or LDC buffer layer. The cell having a SDC buffer layer shows a small degradation in the voltage (0.900–0.897 V) after operating at 1.09 A/cm^2 of the applied current density for 100 h at 973 K. On the contrary, the cell using a LDC buffer layer shows no degradation in the cell voltage when operated at 1.06 A/cm^2 of the current density as shown in Fig. 1(a). Thus, the cell using the LDC buffer layer reveals improved long-term stability compared with the cell using the SDC buffer layer.

https://doi.org/10.1557/jmr.2012.187 Published online by Cambridge University Press

However, the applied current density at 0.9 V in the cell using the LDC buffer layer is lower than that of the cell with the SDC layer. In addition, the cell using the LDC layer shows lower maximum power density (MPD) (1.86 W/cm^2 at 973 K) than that of the cell using the SDC layer (1.99 W/cm^2 at 973 K) as shown in Fig. 1(b). The low performance in the cell with the LDC layer is mainly related with a high IR of the cell compared to that using the SDC buffer layer because the electrical conductivity of LDC is lower than that of SDC. However, the MPD is stable after the long-term operation at 973 K for the cell having LDC buffer layer (1.86–1.84 W/cm^2), while the cell using the SDC buffer layer decreases from 1.99 to 1.90 W/cm^2. The degradation of the MPD in the cell with the SDC buffer layer is attributed to the formation of a secondary phase in the SDC layer and $LaSrGa_3O_7$ phase in the LSGM electrolyte layer during operation.[11,12,24] Therefore, to fabricate a more reliable and powerful metal-supported SOFC, it is necessary to investigate a new buffer layer, which has a higher conductivity than that of LDC and a prior chemical compatibility than that of SDC.

Yamamura et al.[33] and Kim[34] found that codoping led to the increase of the ionic conductivity of doped CeO_2 and the reduction of the activation energy for conduction. Huang et al.[12] reported that 40 mol% LDC had no reactivity with the LSGM, and the La diffusion was originated from the difference of La concentration between the LSGM and LDC. Thus, codoping for LDC was investigated for increasing conductivity. La concentration in the LDC was kept as 40 mol% for maintaining chemical compatibility, and 10 mol% secondary dopant was replaced with the Ce site. Figure 2(a) shows XRD patterns of $Ce_{0.5}La_{0.4}M_{0.1}O_{2-\delta}$ (M = Ga, Y, Pr, Nd, and Sm, denoted as LGC, LYC, LPC, LNC, and LSC, respectively) sintered at 1573 K and a powder mixture consisting of LSGM and $Ce_{0.5}La_{0.4}M_{0.1}O_{2-\delta}$ (1:1 wt%) after sintering at 1623 K [Fig. 2(b)]. The LYC, LPC, and LSC show a typical cubic fluorite structure without any secondary phases as shown in Fig. 2(a). However, the LGC shows a perovskite structure ($LaGaO_3$; JCPDS powder diffraction File No. 83-0566) as secondary phase. The $LaGaO_3$ secondary phase is attributed to the reaction between two dopants (La and Ga) during solid-state reaction. In addition, LYC, LPC, LNC, and LSC show an impurity phase of $LaSrGaO_4$ after calcination at 1623 K for 5 h with

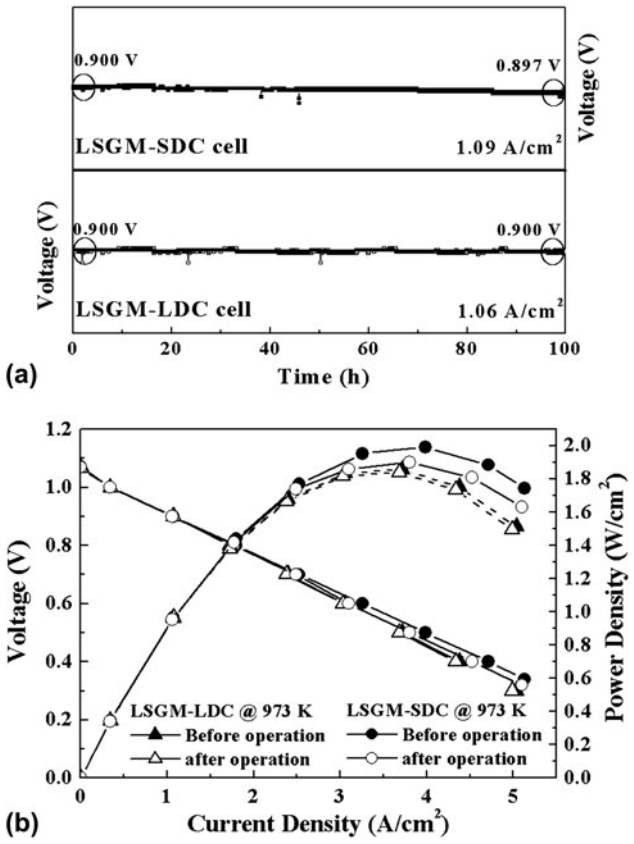


FIG. 1. The power generating property of the metal-supported cell having SDC and LDC buffer layer electrolyte film; (a) long-term performance at 973 K and (b) IV–IP curves.

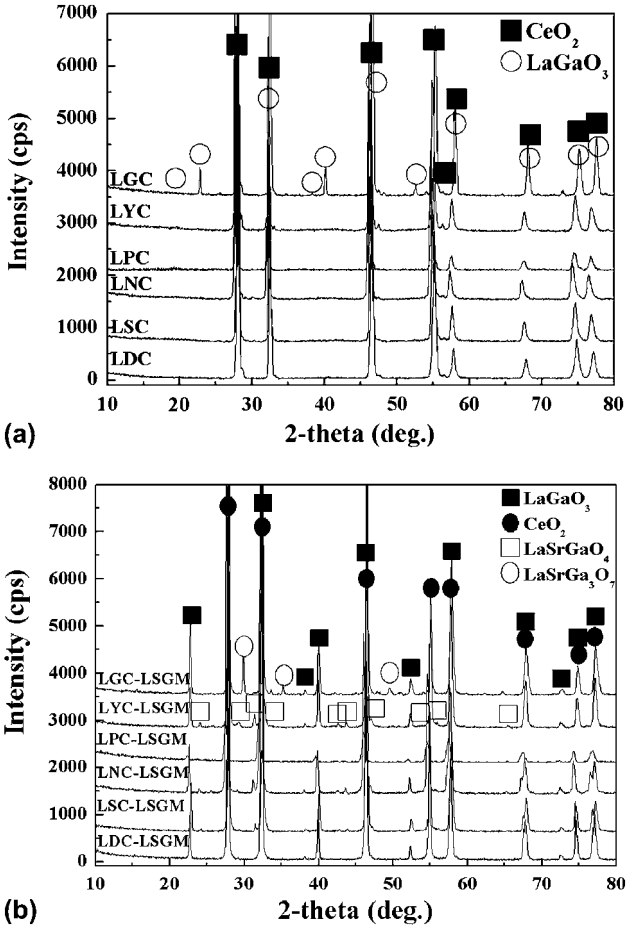


FIG. 2. XRD patterns of (a) $(Ce_{0.5}La_{0.4}M_{0.1})O_{2-\delta}$ and (b) mixtures consisted of LSGM and $(Ce_{0.5}La_{0.4}M_{0.1})O_{2-\delta}$.

https://doi.org/10.1557/jmr.2012.187 Published online by Cambridge University Press

LSGM. Huang et al.[12] reported that the formation of $LaSrGaO_4$ is originated from La diffusion from the LDC buffer layer to the LSGM electrolyte, while the $LaSrGa_3O_7$ phase is formed owing to La deficiency in the LSGM electrolyte caused by the La migration out of the electrolyte. Thus, it is expected that the $LaSrGaO_4$ formation is induced by an excess dopant in the LYC, LPC, LNC, and LSC. On the other hand, the amount of dopant is insufficient in the LGC due to the formation of $LaGaO_3$ during preparation of LGC.

Figure 3 shows the Arrhenius plot for electrical conductivities of codoped LDCs. In the temperature range of 1173–913 K, all codoped LDCs exhibit lower conductivities than that of LDC, although the LPC and LGC show lower activation energies than that of LDC. Thus, codoping LDC ($Ce_{0.5}La_{0.4}M_{0.1}O_{2-\delta}$) is ineffective for improving ionic conductivity and attaining chemical compatibility of LDC.

B. Investigation for alternative materials as buffer layer

An alternative material was investigated for a buffer layer with high compatibility and conductivity for a LSGM electrolyte film. Various oxide materials for buffer layer studied are summarized in Table II. However, all prepared buffer layer materials form some secondary phases after cosintering with either LSGM or NiO at 1623 K for 6 h, except for LPCr ($La_{0.81}Pr_{0.19}CrO_{3-\delta}$), which shows no reactivity against NiO and LSGM as shown in Fig. 4. Therefore, we focused on the investigation for the LPCr as buffer layer. As shown in Fig. 4(a), the sintered composite of LSGM and LPCr shows no secondary phase such as $LaSrGa_3O_7$ and $LaSrGaO_4$. In addition, no impurity or secondary phase is confirmed in the composite of the LPCr and NiO after sintering as shown in Fig. 4(b). Figure 5 shows Arrhenius plot of the electrical conductivity of the LPCr measured by the dc four-probe method in air. The LPCr shows higher conductivity than that of SDC at all temperature ranges. The electrical conductivity of LPCr (0.18 S/cm) is much higher than that of SDC (0.004 S/cm)

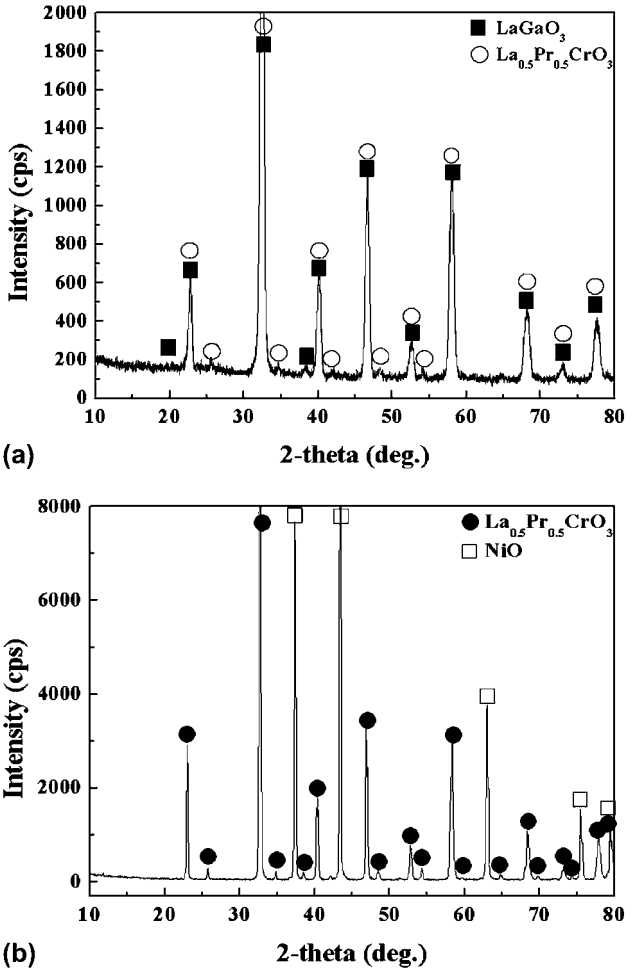


FIG. 4. XRD pattern of a mixture consisting of 19 mol% LPCr and (a) LSGM/(b) NiO after sintering at 1623 K for 6 h.

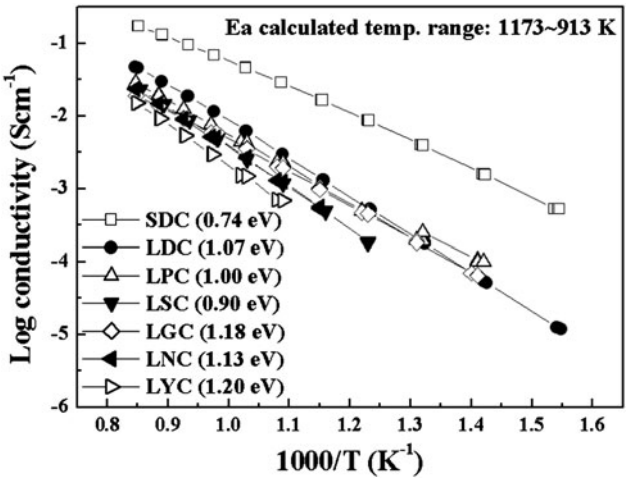


FIG. 3. Arrhenius plot for electrical conductivity of codoped LDC.

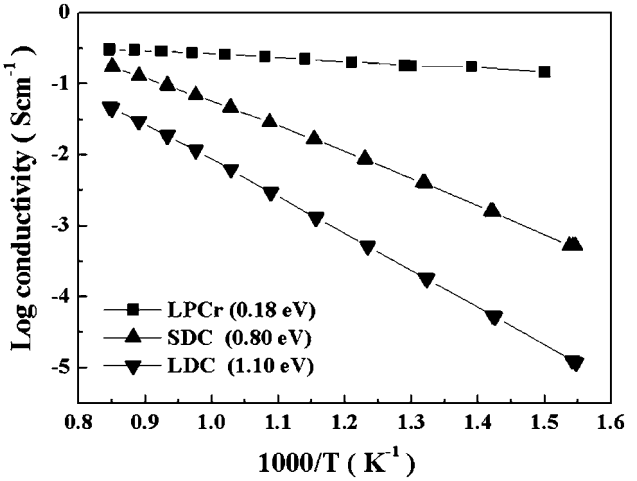


FIG. 5. The Arrhenius plot of conductivity of 19 mol% LPCr and doped CeO_2.

https://doi.org/10.1557/jmr.2012.187 Published online by Cambridge University Press

or LDC (0.0002 S/cm) at 773 K. However, in low oxygen partial pressure at 973 K, the conductivity of LPCr (0.040 S/cm in $P_{O_2} = 10^{-20}$) is similar with that of LDC (0.037 S/cm in $P_{O_2} = 10^{-23}$). As well known, the conductivity of doped CeO_2 increased in low oxygen partial pressure. However, the increased conductivity mainly originated from the enhanced electric conductivity. On the contrary, LPCr shows p-type conduction, and the conductivity decreases with decreasing oxygen partial pressure. In the case of a p-type conductor, in reducing atmosphere ($P_{O_2} < 10^{-8}$), charge compensation is mainly achieved by oxygen vacancy and the electrical transport is mostly ionic.[35] Therefore, it can be expected that the LPCr has higher oxygen ion conductivity in reducing atmosphere than that of LDC. Therefore, the ohmic resistance of a metal-supported SOFC using the LPCr buffer layer may decrease and the power density may increase.

To confirm the power generation property of a metal-supported SOFC with a LPCr buffer layer and LSGM electrolyte films, a thin LPCr film (500 nm) was fabricated on a dense anode substrate by the PLD with an optimized target composition ($La_{0.71}Pr_{0.12}Cr_{1.22}O_3$). A LSGM electrolyte film was then fabricated on the LPCr-deposited film. Figure 6(a) shows XRD pattern of the deposited LSGM–LPCr bilayer electrolyte film after postannealing at 1073 K. The XRD pattern shows NiO and $NiFe_2O_4$ phases from the anode support and typical perovskite peaks of the LSGM and LPCr phases. It reveals that the LPCr buffer layer is successfully fabricated with no detectable formation of secondary phases. Thus, electrochemical performance of the cell using the LPCr buffer layer film was investigated. However, the cell shows a lower OCV than the theoretical value as shown in Fig. 6(b). The OCV is also lower than that of the cell using a SDC or LDC buffer layer. In addition, the MPD of the cell using the LPCr buffer layer is 0.4 W/cm^2 at 973 K, which is smaller than previous results. A low OCV is normally originated from an electronic conduction or gas leakage in electrolyte layer. However, an electronic conduction of the LSGM electrolyte can be ignored because the electrolyte is a pure oxygen ion conductor, and results of SEM–EDX analysis show no detectable interdiffusion of a cation between the LSGM–LPCr bilayer films and Ni–Fe metal substrate after cell test as shown in Fig. 6(c). Thus, an electronic conduction in the LSGM electrolyte can be excluded for the low OCV. Therefore, a gas leakage may be concerned with the low OCV, although the increment of gas leakage in the cell is negligible during operation, and the deposited electrolyte film is relatively dense as shown in Fig. 6(d).

Phase analysis was conducted by XRD measurement for a LPCr film to confirm a reason of the low OCV and power density. Figure 7(a) shows XRD patterns of a LPCr film deposited on the anode substrate before and after

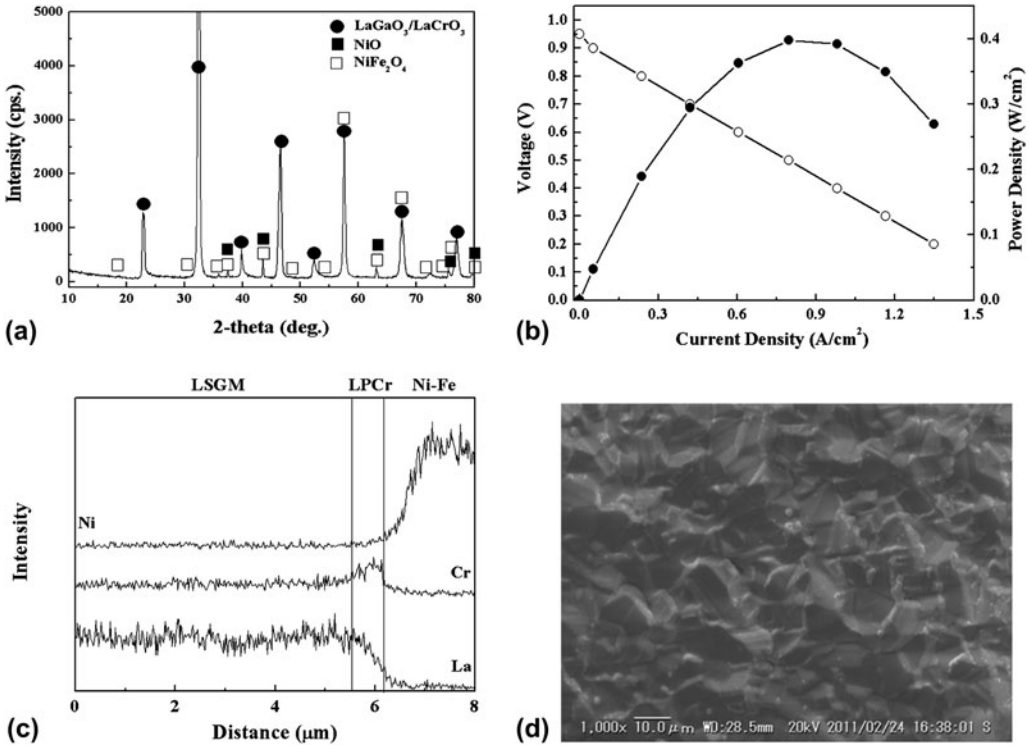


FIG. 6. (a) XRD pattern of the deposited film on NiO–Fe_2O_3, (b) IV–IP curves of the metal-supported cell having LPCr–LSGM bilayer electrolyte at 973 K, (c) the elements distributions of metal-supported cell after testing, and (d) SEM image of deposited film after testing.

https://doi.org/10.1557/jmr.2012.187 Published online by Cambridge University Press

reduction in humidified H_2 atmosphere for 1 h at 973 K. After reduction, no noticeable impurity phase is observed excluding the change of NiO to Ni. However, XRD peaks of the perovskite phase seem to shift toward a higher diffraction angle. The peak shift indicates a change in lattice parameter or composition. As listed in Table IV, the result of EDX analysis suggests that the amount of Pr in the LPCr film decreases after reduction in the humidified H_2. The decrease of Pr content in the LPCr layer may be related with that a Pr(OH) is formed by the reaction of Pr and water as following:

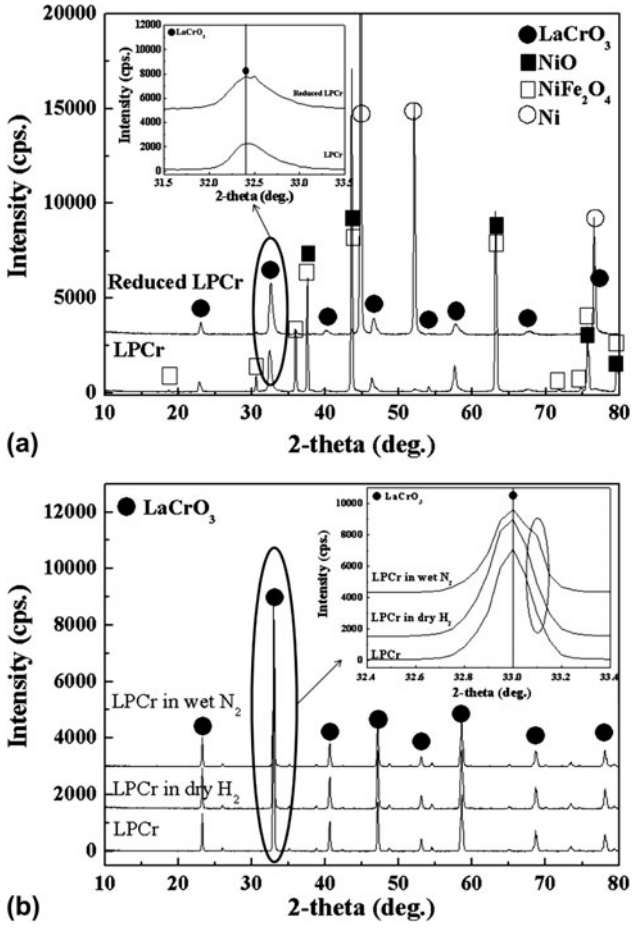


FIG. 7. XRD patterns of (a) deposited LPCr film on NiO–Fe_2O_3 substrate before and after reduction and (b) LPCr disks exposed dry hydrogen and wet nitrogen for 1 h.

TABLE IV. Quantitative analysis of LPCr film before and after reducing the NiO–Fe_2O_3 substrate.

	La		Pr		Cr		
	At.%	Ratio	At.%	Ratio	At.%	Ratio	Total
LPCr film	58.47	...	4.61	...	36.92	...	100.00
Reduced LPCr film	58.64	1.003	4.43	0.961	36.93	1.000	100.00

$$\mathrm{La(Pr)CrO_3 + H_2O(g) \rightarrow Pr(OH)_3\ (or\ La(OH)_3) + La_{1-\alpha}CrO_3 + Cr_2O_3} \quad . (2)$$

Thus, the composition of the LPCr film contacted with the anode may be changed by the reaction since humidified H_2 was supplied into the anode and a small amount of water might be generated by the anode reaction during cell test, resulted in a decrease of the electrical conductivity of the LPCr. To confirm this hypothesis, in which the insufficient performance was caused by the reaction between a LPCr buffer layer and water vapor in the anode environment, the stability of a LPCr film was investigated with XRD analysis after exposing in dry H_2 and humidified N_2 at 973 K. The LPCr exposed in dry H_2 shows no significant change in diffraction patterns as shown in Fig. 7(b). On the other hand, a new but weak peak was appeared at the diffraction angle of $2\theta = 33.15°$ when LPCr was exposed to humidified N_2. At present, the formed crystal phase cannot be assigned; however, this suggests that decomposition of LPCr is not caused by simple reduction but by reaction with humidity. This decomposition of LPCr may result in deterioration of the mechanical strength and electrical conductivity of the LPCr film because of the products of low conductivity of a site-deficient $LaCrO_3$ or Cr_2O_3. Accordingly, the low OCV and power generating performance in the cell using a LPCr buffer layer film may be attributed to the phase decomposition of LPCr layer. Therefore, further detail investigation is requested to use a LPCr buffer layer film in a metal-supported SOFC.

A multilayer electrolyte film, which consisted of LSGM (5 μm), LPCr (300 nm), and SDC (200 nm), was prepared in a metal-supported SOFC using the PLD method. In this cell, the LPCr layer was used for preventing a La migration from the LSGM to SDC, and the SDC layer was intended to prevent the reaction between Pr and water vapor. Figure 8(a) shows the IV–IP curves of the metal-supported cell having the multilayer electrolyte. The cell shows an OCV close to the theoretical value during cell test. It indicates that the mechanical strength of the deposited film is enough to overcome a physical stress originated from the volume change of the metal substrate after reduction and operation temperature change. In addition, the cell shows high maximum power densities 1.98 W/cm^2 at 973 K and 0.53 W/cm^2 at 773 K, which are similar with the values in the cell with a SDC buffer layer film (1.99 W/cm^2 at 973 K and 0.53 W/cm^2 at 773 K). Thus, the power densities suggested that electrochemical performance of the cell using the multilayer electrolyte film including LSGM/LPCr/SDC layers was dominated by the SDC layer, although the electrical conductivity of LPCr was higher than that of SDC. However, a long-term performance was more stable in comparison with the cell having a SDC buffer layer film as shown in Fig. 8(b).

https://doi.org/10.1557/jmr.2012.187 Published online by Cambridge University Press

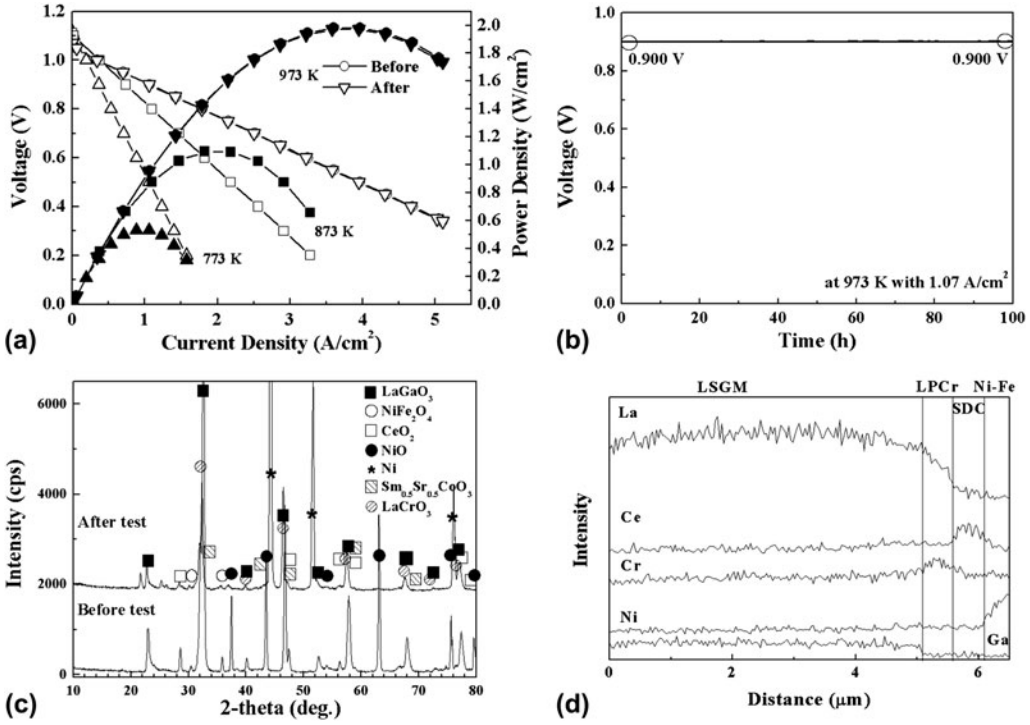


FIG. 8. (a) IV–IP curves and (b) long-term operations at 973 K of the metal-supported cell having SDC–LPCr–LSGM multilayer electrolyte, (c) XRD pattern of the metal-supported cell having LPCr–SDC–LSGM electrolyte, and (d) elements distributions of the metal-supported cell after testing.

The cell with the multilayer film shows no degradation in the cell voltage during the operation at 1.07 A/cm^2 for 100 h at 973 K. This long-term stability suggests that the LPCr layer effectively prevents the La interdiffusion between the LSGM electrolyte and SDC layers, and the SDC layer is also effective for avoiding the Pr(OH) formation during cell operation. XRD [Fig. 8(c)] and EDX [Fig. 8(d)] analysis results evidently reveal that the LPCr layer successfully prevents the La migration from the LSGM electrolyte. Therefore, it is expected that a LPCr can be used as an effective buffer layer for a metal-supported SOFC using a LSGM electrolyte film after preventing the reaction with water vapor.

IV. CONCLUSIONS

Various materials were investigated as a buffer layer for fabricating a reliable metal-supported SOFC using a $LaGaO_3$-based electrolyte thin film. For materials studied, 40 mol% LDC and 19 mol% LPCr showed no reactivity with a LSGM electrolyte and NiO–Fe_2O_3 anode, respectively. A metal-supported cell using the LDC buffer layer showed low power density due to the low conductivity of LDC, while long-term performance of the cell was stable after operation for 100 h. In contrast, when the LPCr was used as buffer layer for a metal-supported SOFC, the cell showed significantly low OCV and power density, which was attributed to the decomposed Pr in the LPCr caused by the reaction with water vapor. However, the metal-supported SOFC using a multilayer electrolyte including LSGM, LPCr, and SDC films showed almost theoretical OCV and high power density, which was similar with that of the cell using a SDC buffer layer, and no degradation in the performance after operation for 100 h at 973 K. Consequently, this study reveals that a LPCr–SDC bilayer is a highly useful buffer layer for a reliable metal-supported SOFC using a LSGM electrolyte film prepared by PLD method.

REFERENCES

1. O. Yamamoto: Solid oxide fuel cells: Fundamental aspects and prospects. *Electrochim. Acta* **45**, 2423 (2000).
2. S.C. Singhal: Solid oxide fuel cells for stationary, mobile, and military applications. *Solid State Ionics* **152–153**, 405 (2002).
3. N.Q. Minh: Solid oxide fuel cell technology – features and applications. *Solid State Ionics* **174**, 271 (2004).
4. H. Yahiro, Y. Baba, K. Eguchi, and H. Arai: High temperature fuel cell with ceria-yttria solid electrolyte. *J. Electrochem. Soc.* **135**, 2077 (1988).
5. A.V. Virkar: Theoretical analysis of solid oxide fuel cells with two-layer, composite electrolytes: Electrolyte stability. *J. Electrochem. Soc.* **138**, 1481 (1991).
6. M. Mogensen, N.M. Sammes, and G.A. Tompsett: Physical, chemical and electrochemical properties of pure and doped ceria. *Solid State Ionics* **129**, 63 (2000).
7. T. Ishihara, H. Matsuda, and Y. Takita: Doped $LaGaO_3$ perovskite type oxide as a new oxide ionic conductor. *J. Am. Chem. Soc.* **116**, 3801 (1994).
8. T. Ishihara, H. Minami, H. Matsuda, H. Nishiguchi, and Y. Takita: Decreased operating temperature of solid oxide fuel cells (SOFCs)

https://doi.org/10.1557/jmr.2012.187 Published online by Cambridge University Press

by the application of $LaGaO_3$-based oxide as electrolyte. *Chem. Commun.* **8**, 929 (1996).
9. T. Ishihara, M. Honda, T. Shibayama, H. Minami, H. Nishiguchi, and Y. Takita: Intermediate temperature solid oxide fuel cells using a new $LaGaO_3$ based oxide ion conductor. *J. Electrochem. Soc.* **145**, 3177 (1998).
10. M. Feng, J.B. Goodenough, K. Huang, and C. Milliken: Fuel cells with doped lanthanum gallate electrolyte. *J. Power Sources* **63**, 47 (1996).
11. K. Huang, R. Tichy, and J.B. Goodenough: Superior perovskite oxide-ion conductor; strontium-and magnesium-doped $LaGaO_3$: I, phase relationships and electrical properties. *J. Am. Ceram. Soc.* **81**, 2565 (1998).
12. K. Huang, J.H. Wan, and J.B. Goodenough: Increasing power density of LSGM-based solid oxide fuel cells using new anode materials. *J. Electrochem. Soc.* **148**, A788 (2001).
13. Z.H. Bi, B.L. Yi, W. Wang, Y.L. Dong, Y.C. Wu, Y.C. She, and M.J. Cheng: A high-performance anode-supported SOFC with LDC-LSGM bilayer electrolytes. *Electrochem. Solid-State Lett.* **7**, A105 (2004).
14. D.Y. Lee, J.H. Han, E.G. Kim, R.H. Song, and D.R. Shin: Performance of strontium- and magnesium-doped lanthanum gallate electrolyte with lanthanum-doped ceria as a buffer layer for IT-SOFCs. *J. Power Sources*, **185**, 207 (2008).
15. J.W. Yan, Z.G. Lu, Y. Jiang, Y.L. Dong, Y.C. Yu, and W.Z. Li: Fabrication and testing of a doped lanthanum gallate electrolyte thin-film solid oxide fuel cell. *J. Electrochem. Soc.* **149**, A1132 (2002).
16. T. He, Q. He, L. Pei, and Y. Ji: Doped lanthanum gallate film solid oxide fuel cells fabricated on a Ni/YSZ anode support. *J. Am. Ceram. Soc.* **89**, 2664 (2006).
17. W. Guo, J. Liu, and Y. Zhang: Electrical and stability performance of anode-supported solid oxide fuel cells with strontium- and magnesium-doped lanthanum gallate thin electrolyte. *Electrochim. Acta* **53**, 4420 (2008).
18. F. Bozza, R. Polini, and E. Traversa: High performance anode-supported intermediate temperature solid oxide fuel cells (IT-SOFCs) with $La_{0.8}Sr_{0.2}Ga_{0.8}Mg_{0.2}O_{3-\delta}$ electrolyte films prepared by electrophoretic deposition. *Electrochem. Commun.* **11**, 1680 (2009).
19. J.W. Yan, H. Matsumoto, M. Enoki, and T. Ishihara: High-power SOFC using $La_{0.9}Sr_{0.1}Ga_{0.8}Mg_{0.2}O_{3-\delta}$ composite film. *Electrochem. Solid-State Lett.* **8**, A389 (2005).
20. T. Ishihara, J.W. Yan, M. Shinagawa, and H. Matsumoto: Ni-Fe bimetallic anode as an active anode for intermediate temperature SOFC using $LaGaO_3$ based electrolyte film. *Electrochim. Acta* **52**, 1645 (2006).
21. Y.W. Ju, H. Matsumoto, T. Ishihara, T. Inagaki, and H. Eto: Preparation of $LaGaO_3$ based oxide thin film on porous Ni-Fe metal substrate and its SOFC application. *J. Korean Chem. Soc.* **45**, 796 (2008).
22. Y.W. Ju, H. Eto, T. Inagaki, and T. Ishihara: High power SOFC using LSGM film on NiFe porous bi-metal substrate. *ECS Trans.* **25**, 719 (2009).
23. Y.W. Ju, H. Eto, T. Inagaki, and T. Ishihara: Preparation of Ni-Fe bimetallic porous anode support for SOFCs using $LaGaO_3$ based electrolyte film with high power density. *J. Power Sources* **195**, 6294 (2010).
24. Y.W. Ju, T. Inagaki, S. Ida, and T. Ishihara: Sm(Sr)CoO_3 cone cathode on $LaGaO_3$ thin film electrolyte for with IT-SOFC high power density. *J. Electrochem. Soc.* **158**, 1 (2011).
25. N.Q. Minh, T.R. Armstrong, J.R. Esopa, J.V. Guiheen, C.R. Home, and J.J. van Ackeren: Proceedings of the third international symposium on the solid oxide fuel cell. *Electrochem. Soc. Proc.* **93–94**, 801 (1993).
26. R. Yamaguchi, K. Hashimoto, H. Sakata, H. Kajiware, K. Watanable, T. Setiguchi, K. Eguchi, and H. Arai: Proceedings of the third international symposium on the solid oxide fuel cell. *Electrochem. Soc. Proc.* **93–94**, 704 (1993).
27. C.C. Chen, M.M. Nasrallah, and H.U. Anderson: Synthesis and characterization of YSZ thin film electrolytes. *Solid State Ionics* **71**, 101 (1994).
28. S. de Souza, S.J. Visco, and L.C. De Jonghe: Thin film solid oxide fuel cell with high performance at low-temperature. *Solid State Ionics* **98**, 57 (1997).
29. C. Lunot and Y. Denos: Evaluation of Different Processes to Fabricate Thin Film Solid Fuel Cells, in *Proceeding of the 1998 International Gas Research Conference, San Diego, California, November 8-11, 1998*; D.A. Dolenc, ed., Gas Research Institute: Chicago, IL, 1998; p. 834.
30. C.J. Li, C.X. Li, Y.Z. Xing, M. Gao, and G.J. Yang: Influence of YSZ electrolyte thickness on the characteristics of plasma-sprayed cermet supported tubular SOFC. *Solid State Ionics* **177**, 2065 (2006).
31. W. Bai, K.L. Choy, R.A. Rudkin, and B.C.H. Steele: The process, structure and performance of pen cells for the intermediate temperature SOFCs. *Solid State Ionics* **113–115**, 259 (1998).
32. L.S. Wang, E.S. Thiele, and S.A. Barnett: Sputter deposition of yttria-stabilized zirconia and silver cermet electrodes for SOFC applications. *Solid State Ionics* **52**, 261 (1992).
33. H. Yamamura, E. Katoh, M. Ichikawa, K. Kakinuma, M. Tori, and H. Haneda: Multiple doping effect on the electrical conductivity in the $(Ce_{1-x-y}La_xM_y)O_{2-\delta}$ (M = Ca, Sr) system. *Electrochemistry* **68**, 455 (2000).
34. D.J. Kim: Lattice parameters, ionic conductivities, and solubility limits in fluorite-structure MO_2 oxide (M = Hf^{4+}, Zr^{4+}, Ce^{4+}, Th^{4+}, U^{4+}) solid solutions. *J. Am. Ceram. Soc.* **72**, 1415 (1989).
35. L.L. Zhang: *Doped $LaCrO_3$ as Interconnect in SOFC*. (Ohio State Literature Review, Columbus, OH, 2004).

https://doi.org/10.1557/jmr.2012.187 Published online by Cambridge University Press